Superconductivity induced by Mg deficiency in noncentrosymmetric phosphide Mg_2Rh_3P

Akira Iyo,[1,*] Izumi Hase,[1] Hiroshi Fujihisa,[1] Yoshito Gotoh,[1] Nao Takeshita,[1] Shigeyuki Ishida,[1] Hiroki Ninomiya,[1] Yoshiyuki Yoshida,[1] Hiroshi Eisaki,[1] and Kenji Kawashima[1,2]

[1]*National Institute of Advanced Industrial Science and Technology (AIST), 1-1-1 Umezono, Tsukuba, Ibaraki 305–8568, Japan*

[2]*IMRA Material R&D Co., Ltd., 2-1 Asahi-machi, Kariya, Aichi 448-0032, Japan*

(Received 8 July 2019; revised manuscript received 20 September 2019; published 26 December 2019)

The search for noncentrosymmetric superconductors that may exhibit unusual physical properties and unconventional superconductivity has yielded the synthesis of a noncentrosymmetric phosphide Mg_2Rh_3P with an Al_2Mo_3C-type structure. Although stoichiometric Mg_2Rh_3P does not exhibit superconductivity at temperatures above 2 K, we found that an Mg deficiency of approximately 5 at.% in the Mg_2Rh_3P-induced superconductivity at 3.9 K. Physical properties such as the lattice parameter $a = 7.0881$ Å, Sommerfeld constant $\gamma_n = 5.36\,\mathrm{mJ\,mol^{-1}\,K^{-2}}$, specific heat jump $\Delta C_{el}/\gamma_n T_c = 0.72$, electron–phonon coupling constant $\lambda_{e\text{-}p} = 0.58$, upper critical field $H_{c2}(0) = 24.3$ kOe, and pressure effect $dT_c/dP = -0.34$ K/GPa were measured for the superconducting $Mg_{2-\delta}Rh_3P$ ($\delta \sim 0.1$). Band-structure calculations indicate that exotic fermions, which are not present in high-energy physics, exist in Mg_2Rh_3P. Since Mg, Rh, and P are the first elements used at each crystal site of Al_2Mo_3C-type compounds, the discovery of Mg_2Rh_3P may guide the search for new related materials.

DOI: 10.1103/PhysRevMaterials.3.124802

I. INTRODUCTION

Noncentrosymmetric superconductors (NCS) whose crystal structures lack inversion symmetry have attracted significant attention because of their potential as a platform for novel physical phenomena, as well as the possibility for unconventional superconductivity. [1,2] Besides the exploration of intriguing physical properties, it is also important to expand the variety of NCS compounds. Compounds of the form A_2M_3X, with an Al_2Mo_3C-type structure ($P4_132$, space group no. 213), do not have inversion symmetry. Figure 1 shows the schematic crystal structure of the A_2M_3X compound type. Its structure consists of a three-dimensional network of corners sharing M_6X octahedrons. The M_6X octahedrons are significantly distorted because two A atoms are located in the space surrounded by the octahedrons. When one A atom occupies the space, the structure becomes a so-called "antiperovskite AXM_3" that typically has the Pm-3m space group.

Compounds (a)–(g) in Table I are Al_2Mo_3C-type superconductors identified before this study. These superconductors are attractive in terms of both theoretical physics and application-based perspectives. The superconducting state of Li_2Pt_3B has been shown to include a spin-triplet component by nuclear magnetic resonance (NMR) spectroscopy [3], while Li_2Pd_3B appears to be spin-singlet. Al_2Mo_3C is a strong-coupled superconductor that deviates from Bardeen–Cooper–Schrieffer (BCS)-type behavior [4], with a relatively high critical temperature ($T_c = 9.3$ K) and high upper critical field $H_{c2}(0)$(=150 kOe) [5]. Moreover, the A_2M_3X crystal structure is attracting interest, as it has been shown that a new type of quasiparticle referred to as an exotic fermion exists in Li_2Pd_3B [6]. This new type of quasiparticle may provide a novel platform for topological quantum devices.

As shown in Table I(a)–(g), the M site in A_2M_3X superconductors is occupied by a 4d–5d transition metal (=Nb, Mo, Pd, Re, or Pt) from various element groups. In addition, the A(=Li, Al, Cr, Rh, Ag) and X(=B, C, N, S) sites accept various elements from a wide range of element groups. This indicates that the A_2M_3X ternary system is flexible in terms of the combination of the three constituent elements, and still presents possibilities for exploring new superconductors.

We tested several possible combinations of A, M, and X from a wide range of element groups, and consequently succeeded in synthesizing the new Al_2Mo_3C-type phosphide Mg_2Rh_3P. Though stoichiometric Mg_2Rh_3P did not show superconductivity, we found that superconductivity was induced in Mg_2Rh_3P by Mg deficiency, as listed in Table I(h). In this paper, we first describe the synthesis conditions of non-superconducting stoichiometric samples (NS-Mg_2Rh_3P) and superconducting Mg-deficient samples (SC-$Mg_{2-\delta}Rh_3P$). We then experimentally evaluate the refined crystal structures and basic physical properties of the samples, such as magnetization, resistivity, specific heat, and pressure effects. Finally, we address the existence of the above-mentioned exotic fermions in Mg_2Rh_3P using theoretical calculations.

II. MATERIAL SYNTHESIS

Control of Mg (vapor) concentration during the sample synthesis was necessary to control the superconductivity and quality of the Mg_2Rh_3P samples. We propose the following method for sample synthesis.

An Rh powder was ground with a P chunk using a mortar in a glove box. The powder, with a nominal composition of Rh_3P, was pressed into pellet form (~0.2 g) and sealed in an evacuated quartz tube (8 mm in inner diameter and 80 mm in length) with a certain molar ratio of Mg chips (~1 mm in size) as described below. The temperature of the quartz

*iyo-akira@aist.go.jp

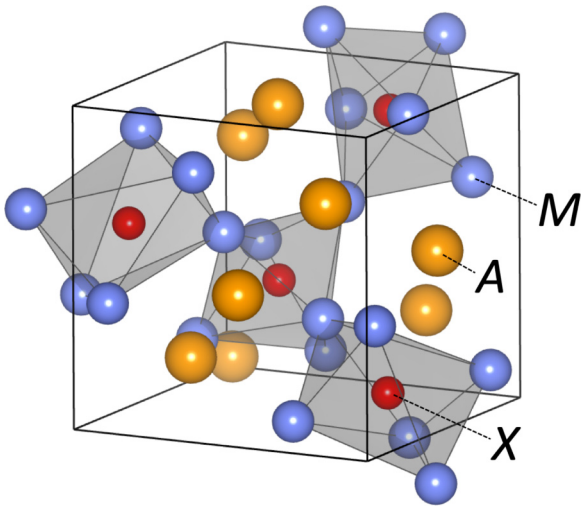

FIG. 1. Schematic of the A_2M_3X (Al_2Mo_3C-type) crystal structure, produced using the VESTA software [7]. Thick solid lines indicate the unit cell.

tube was raised from room temperature to 875–925 °C for 2 h and maintained for 8–16 h. During the heat treatment, Mg vapor was generated inside the quartz tube and reacted with both the pellet and the quartz tube. The Mg vapor eventually disappeared when the reactions between the Mg and the pellet and quartz tube were completed.

As discussed in more detail below, the superconductivity of Mg_2Rh_3P was induced by Mg deficiency. Both the Mg deficiency and sample quality depended on the quantity of the Mg chips, heating temperature and time, and also possibly the inner dimensions of the quartz tube. If the quantity of Mg chips was large enough, *e.g.*, with a molar ratio of Mg to Rh_3P of approximately 8–10 (0.115–0.143 g Mg chips for the 0.2 g Rh_3P pellet), a nonsuperconducting sample was obtained because the sample was exposed to Mg vapor for the entire heat-treatment period.

The molar ratio of Mg to Rh_3P, heating temperature, and treatment time of 5 (0.072 g Mg chips for the 0.2 g Rh_3P pellet), 925 °C, and 16 h, respectively, provided the best conditions for obtaining a superconducting sample. Impurity phases formed by the decomposition of Mg_2Rh_3P were then observed at the surface of the superconducting pellet, while significant decomposition was not observed in the case of the nonsuperconducting sample. It appears that the Mg deficiency was introduced from the surface of the pellet after the Mg vapor pressure was decreased. Thus, the presence of a decomposed surface is an indicator of a superconducting pellet. These results suggest that the decomposition of Mg_2Rh_3P most likely occurs when the Mg deficiency exceeds a certain upper limit.

TABLE I. Superconductors with the Al_2Mo_3C-type structure reported in the literature, and the $Mg_{2-\delta}Rh_3P$ superconductor synthesized in this study.

	Compounds	T_c (K)	a (Å)	$H_{c2}(0)$(kOe)	Ref.
(a)	Al_2Mo_3C	9.3	6.87	150	[8,4,5]
(b)	Al_2Nb_3N	1.3	7.03	–	[9]
(c)	Ag_2Pd_3S	2.25	7.23	6.3	[10,11]
(d)	Li_2Pd_3B	8	6.75	50	[12,13]
(e)	Li_2Pt_3B	2.8	6.76	20	[13,14]
(f)	Cr_2Re_3B	4.8	6.61	100	[15]
(g)	Rh_2Mo_3N	4.3	6.81	74.1	[16]
(h)	$Mg_{2-\delta}Rh_3P$	3.9	7.09	24.3	[a]

[a]This study.

III. EXPERIMENTS AND METHODS

Powder x-ray diffraction (XRD) patterns were obtained at room temperature using a diffractometer (Rigaku, Ultima IV) with Cu$K\alpha$ radiation. Crystal structures of the samples were refined via Rietveld analysis using BIOVIA Materials Studio Reflex software (version 2018 R2) [17]. Magnetization (M) measurements were performed under magnetic fields (H) using a magnetic-property measurement system (Quantum Design, MPMS-XL7). Electrical resistivity and specific heat (C) were measured by the four-probe method, using a physical-property measurement system (Quantum Design, PPMS). The compositions of the samples were analyzed by energy-dispersive x-ray (EDX) spectrometry (Oxford, SwiftED3000) using an electron microscope (Hitachi High-Technologies, TM3000). The T_c was measured under pressures of up to 1.5 GPa using a piston-cylinder pressure cell (Electro Lab, MLPC-15). Daphne oil 7373 was used as a pressure-transmitting medium. The applied pressure was determined by a Pb manometer that was placed adjacent to the sample.

First-principles electronic band structure calculations were also performed using the full-potential linearized augmented plane-wave method and generalized gradient approximation for the exchange-correlation potential [18,19]. Spin-orbit interaction was included in the calculations. Details of our calculations are provided in a previous work [20].

IV. RESULTS AND DISCUSSION

The experimental results were obtained for NS-Mg_2Rh_3P and SC-$Mg_{2-\delta}Rh_3P$ synthesized with Mg:Rh_3P molar ratios, heating temperatures, and heating times of 8, 875 °C, and 10 h and 5, 925 °C and 16 h, respectively. The decomposed surface of the SC-$Mg_{2-\delta}Rh_3P$ pellet was removed prior to the measurements. Both samples were silver in color and stable in ambient air.

A. Composition

In order to elucidate the difference in superconductivity, the sample compositions were analyzed by EDX spectrometry. The composition ratio was determined by averaging the data from approximately thirty spots on the polished sample surfaces. In this manner, the obtained composition ratios for Mg:Rh:P were 1.90 (4):3.00 (4):1.04 (2) for SC-$Mg_{2-\delta}Rh_3P$, and 2.00 (4):3.00 (4):1.06 (1) for NS-Mg_2Rh_3P. SC-$Mg_{2-\delta}Rh_3P$ was found to have an Mg deficiency of approximately 5 at.% ($\delta \sim 0.1$), while NS-Mg_2Rh_3P had a nearly stoichiometric composition ratio (Mg : Rh : P = 2 : 3 : 1). Considering the synthesis conditions of the samples, these results are in line with the expectations. It is likely that Mg_2Rh_3P

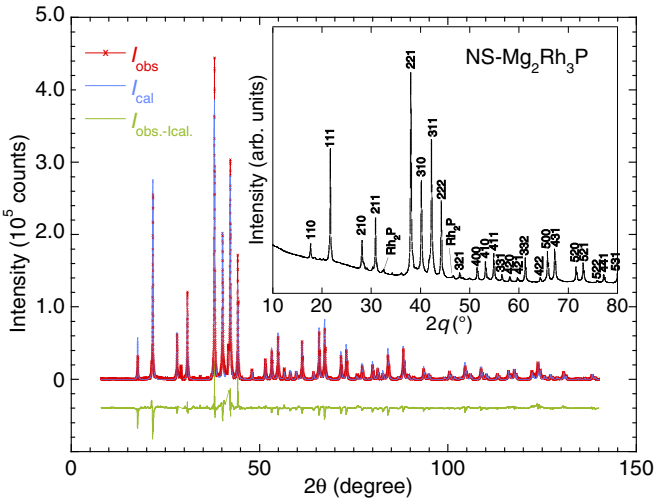

FIG. 2. Powder XRD pattern and Rietveld fitting for NS-Mg_2Rh_3P. $I_{obs.}$ and $I_{cal.}$ indicate the observed and calculated diffraction intensities, respectively. Inset: magnification diffraction angles $2\theta = 10 - 80^\circ$, with a diffraction index for each peak.

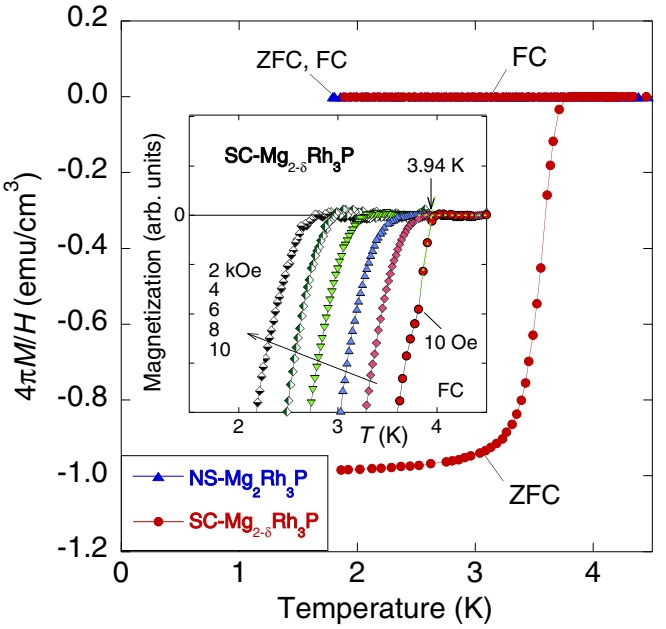

FIG. 3. T dependence of $4\pi M/H$ for NS-Mg_2Rh_3P and SC-$Mg_{2-\delta}Rh_3P$. Measurements were performed with zero-field-cooling (ZFC) and field-cooling (FC) modes. Inset shows T dependence of FC magnetization for SC-$Mg_{2-\delta}Rh_3P$ under magnetic fields up to 10 kOe. Backgrounds were subtracted from the data.

decomposes when the Mg deficiency exceeds ∼5 at.% (upper limit for Mg deficiency).

B. Crystal structure

The XRD patterns of NS-Mg_2Rh_3P and SC-$Mg_{2-\delta}Rh_3P$ were similar and could not be distinguished at a glance. Figure 2 shows the XRD pattern and Rietveld fitting for NS-Mg_2Rh_3P. The sample is nearly monophasic and its diffraction pattern is well fitted by assuming the Al_2Mo_3C-type structure. Small peaks from Rh_2P are observed in the diffraction pattern. The results of Rietveld structure refinements for NS-Mg_2Rh_3P and SC-$Mg_{2-\delta}Rh_3P$ are summarized in Table II. SC-$Mg_{2-\delta}Rh_3P$ has a slightly smaller lattice parameter than NS-Mg_2Rh_3P, which may arise from the Mg deficiency. Note that the Mg deficiency is too small to be detected by Rietveld analysis.

The space group is either $P4_132$ (Cubic, no. 213) or its enantiomorph, $P4_332$ (Cubic, no. 212). The occupancy is fixed to 1 at all atomic sites. The atomic coordinates of Mg, Rh, and P are (x, x, x), $(1/8, y, y + 1/4)$, and $(3/8, 3/8, 3/8)$, respectively, while global isotropic temperature factors for all atoms are employed in both refinements. The mean-square displacements $U_{iso}(Å^2)$ are 0.024(1) and 0.025(1) for all atomic sites for NS-Mg_2Rh_3P and SC-$Mg_{2-\delta}Rh_3P$, respectively.

TABLE II. Results of Rietveld structure refinements for NS-Mg_2Rh_3P and SC-$Mg_{2-\delta}Rh_3P$ at room temperature.

	NS-Mg_2Rh_3P	SC-$Mg_{2-\delta}Rh_3P$
a (Å)	7.0900(1)	7.0881(1)
V (Å^3)	356.35(2)	356.11(2)
x	0.0397(2)	0.0403(2)
y	0.1818(1)	0.1823(1)
$l_{P\text{-}Rh}$(Å)	2.276 (1)	2.274 (1)
R_{wp}(%)	13.10	14.00
R_e(%)	9.05	11.03
S	1.45	1.27

C. Superconductivity

Figure 3 shows the temperature (T) dependence of $4\pi M/H$ for NS-Mg_2Rh_3P and SC-$Mg_{2-\delta}Rh_3P$. NS-Mg_2Rh_3P shows a trace of superconductivity, which is not visible in Fig. 3. The small superconducting component is owing to the Mg deficiency in part of the polycrystalline Mg_2Rh_3P. However, a significant superconducting transition is observed for SC-$Mg_{2-\delta}Rh_3P$, with an onset T_c of 3.94 K. The shielding volume fraction is calculated to be 98% at 2 K considering the demagnetizing effect. The volume fraction is large enough for the compound to be regarded as a bulk superconductor. The T dependence of the magnetization under magnetic fields up to 10 kOe is shown in the inset of Fig. 3. T_c is decreased with increasing applied magnetic field.

The effect of Mg deficiency on superconductivity has previously been discussed by Hase *et al.* on the basis of electronic band structure calculations [20]. Their work indicated that the density of states (DOS) of NS-Mg_2Rh_3P decreased at the Fermi level E_F, and that the value of the DOS was very small at E_F. Mg deficiency was shown to cause holes in the valence band and the consequent shift of E_F drastically increased the DOS. Thus, the experimental result that only Mg-deficient Mg_2Rh_3P shows superconductivity may be explained in terms of an increase in the DOS.

Figure 4 shows the T dependence of resistivity for NS- and SC-$Mg_{2-\delta}Rh_3P$. Both samples exhibit similar metallic T-dependent resistivity in the normal state. The residual

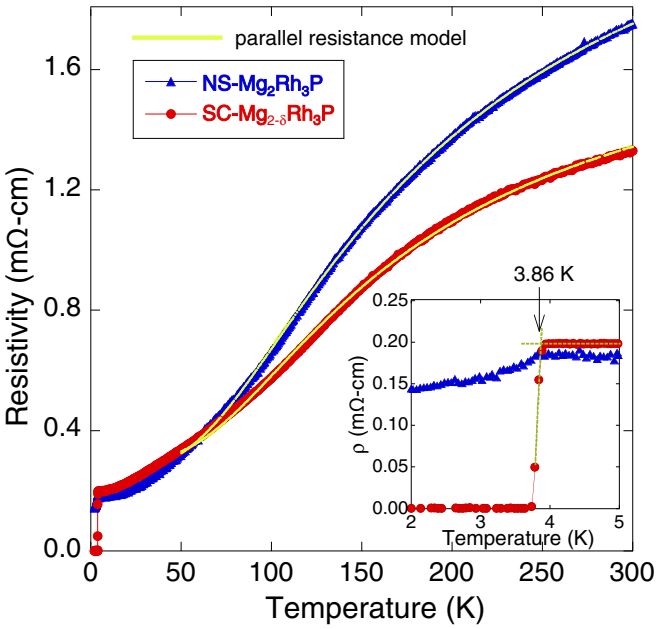

FIG. 4. T dependence of resistivity for NS-Mg_2Rh_3P and SC-$Mg_{2-\delta}Rh_3P$. The inset shows an enlargement near the superconducting transition temperature. The yellow curves show fitting using the parallel resistance model.

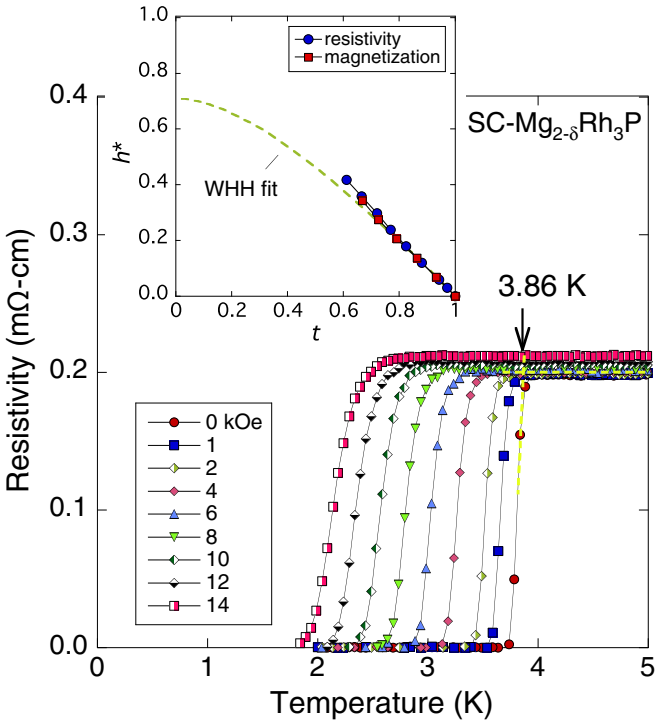

FIG. 5. T dependence of the resistivity as a parameter of magnetic field strengths up to 14 kOe for SC-$Mg_{2-\delta}Rh_3P$. The T_c was defined by the onset of transition. The inset shows the $t(=T/T_c)$ dependent reduced upper critical field h^*. The dashed curve indicates WHH fitting.

resistance ratio $\rho(300\ \mathrm{K})/\rho(\sim 0\ \mathrm{K})$ of SC-$Mg_{2-\delta}Rh_3P$ is smaller than that of NS-Mg_2Rh_3P, which can be explained by carrier scattering resulting from the Mg deficiency of SC-$Mg_{2-\delta}Rh_3P$. As shown in the inset of Fig. 4, only SC-$Mg_{2-\delta}Rh_3P$ indicates a clear superconducting transition at the onset T_c of 3.86 K, close to the value measured through magnetization tests. NS-Mg_2Rh_3P shows only a small decrease in resistivity below approximately 3.8 K, because of a low-content superconducting component detected by the magnetization measurement.

To approximate the Debye temperature Θ_D, we fitted $\rho(T)$ above 50 K using the parallel resistance model $1/\rho(T) = 1/\rho_{BG}(T) + 1/\rho_{max}$ [21], where $\rho_{BG}(T)$ and ρ_{max} are the Bloch–Grüneisen term and saturation resistivity, respectively. Fits employing this model are shown in Fig. 4 as yellow curves, revealing $\Theta_D = 335$ K and 357 K for NS-Mg_2Rh_3P and SC-$Mg_{2-\delta}Rh_3P$, respectively. Note that the resistivity below 50 K cannot be fitted with this model.

The T dependence of the resistivities under magnetic fields up to 14 kOe is shown in Fig. 5 for SC-$Mg_{2-\delta}Rh_3P$. T_c decreases with an increasing applied magnetic field and a small magnetoresistance is observed. The T dependence of the upper critical magnetic field H_{c2} was obtained by defining the onset transitions of resistivity and magnetization, as shown in Figs. 5 and 3, respectively. The H_{c2} values obtained from both measurements show good agreement.

The inset of Fig. 5 shows the reduced critical field $h^*(=-H_{c2}/(dH_{c2}/dt)_{t=1})$ versus $t(=T/T_c)$ [22,23]. The value of h^* changes almost linearly, and no saturation is observed in the measured temperature range. SC-$Mg_{2-\delta}Rh_3P$ is presumed to be a weak-coupling BCS-type superconductor with an experimentally evaluated small $\lambda_{e\text{-}p}$ ($\sim$0.58), as discussed in the next subsection. Werthamer–Helfand–Hohenberg (WHH) theory [22,23] was used to fit the data. The WHH fit is indicated by the dashed curve in the inset of the figure. $H_{c2}(0)$ is estimated to be 24.3 kOe using $H_{c2}(0) = 0.69T_c(dH_{c2}/dT)_{T_c}$ (dirty limit). This H_{c2} (0) is considerably smaller than the Pauli limit H_P ($=1.86 \times T_c$) of $\sim$70 kOe [24,25], suggesting that the upper critical field is limited by orbital pair breaking (Maki parameter $\alpha_M < 1/\sqrt{2}$ [26]) in SC-$Mg_{2-\delta}Rh_3P$. If we examine the behavior of H_{c2} in more detail, H_{c2} appears to deviate slightly upward from the WHH curve below $t \sim 0.8$. Such behavior is also observed in some NSCs [11,27,28]. To obtain a more detailed analysis, measurements of H_{c2} at lower temperatures (<2 K) are necessary.

The Ginzburg–Landau coherence length ξ_0 is calculated to be 116 Å employing $H_{c2}(0) = \Phi_0/2\pi{\xi_0}^2$, where Φ_0 is the magnetic flux quantum.

Figure 6 shows the magnetization (M–H) curves at various temperatures below T_c for SC-$Mg_{2-\delta}Rh_3P$. The M–H curves exhibit the typical behavior of type-II superconductors. To estimate the lower critical field H_{c1}, first, the H_x is defined for each M–H curve, as shown representatively for the M–H curve at 2 K in Fig. 6. Then H_{c1} is calculated by considering a demagnetization factor N estimated to be 0.10 from the size of the measured sample, namely, $H_{c1} = H_p/(1\text{-}N)$. The inset of Fig. 6 depicts the thus-obtained H_{c1} as a function of $(T/T_c)^2$. On the basis of GL theory $H_{c1}(T) = H_{c1}(0)[1\text{-}(T/T_c)^2]$, we derive $H_{c1}(0)$ to be 72.7 Oe. The London penetration depth of $\lambda_0 = 3010$ Å is calculated using an approximation of $H_{c1}(0) = \Phi_0/\pi{\lambda_0}^2$. The GL parameter of $\kappa_{GL} = \lambda_0/\xi_0$ is

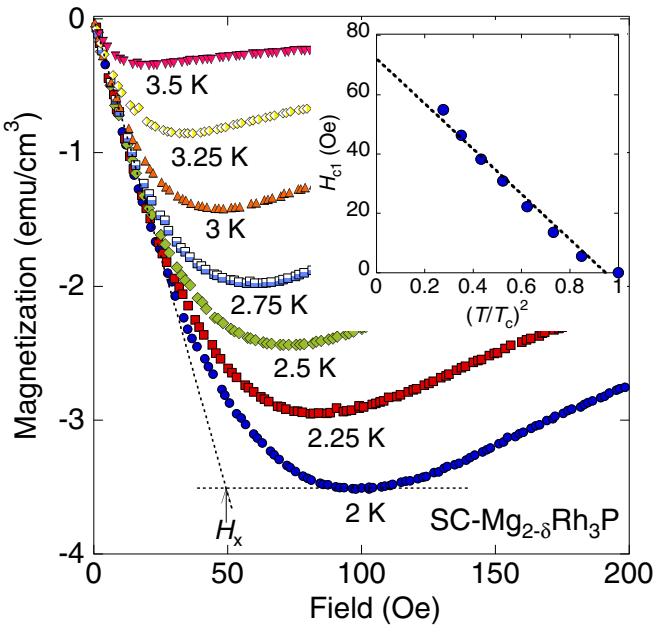

FIG. 6. Field dependence of magnetization at various temperatures below T_c for SC-$Mg_{2-\delta}Rh_3P$. Inset shows H_{c1} as a parameter of $(T/T_c)^2$. The dashed line in the inset is a linear fitting of the data.

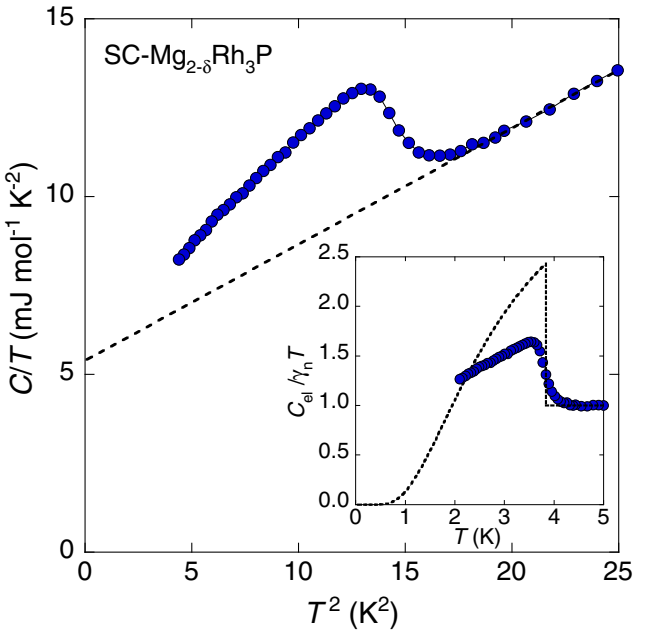

FIG. 7. C/T vs. T^2 of SC-$Mg_{2-\delta}Rh_3P$ below 5 K. The dotted line shows the fitting of data for $T = 4.2 - 5$ K with $C/T = \gamma_n + \beta T^2$ and its extrapolation to $T = 0$. Inset shows the temperature dependence of $C_{el}/\gamma_n T$. The $C_{el}/\gamma_n T$ below T_c predicted by the BCS theory is shown as a dashed curve.

determined to be 26, which is an appropriate value ($>1/\sqrt{2}$) for a type-II superconductor.

D. Specific heat

Figure 7 shows the T^2 dependence of C/T for SC-$Mg_{2-\delta}Rh_3P$ at $H = 0$. The data in the temperature range between 4.2–5 K is fitted with $C/T = \gamma_n + \beta T^2$, where γ_n (the Sommerfeld constant) and β are coefficients related to the electron and phonon contributions to the total specific heat ($C = C_{el} + C_{ph}$), respectively. The fitting yields values of $\gamma_n = 5.36\,\mathrm{mJ\,mol^{-1}\,K^{-2}}$ and $\beta = 0.328\,\mathrm{mJ\,mol^{-1}\,K^{-4}}$. The corresponding value of γ_n for stoichiometric NS-Mg_2Rh_3P obtained by band-structure calculation was $1.41\,\mathrm{mJ\,mol^{-1}\,K^{-2}}$ [20]. This value is much smaller than the experimental result, which supports the concept that Mg deficiency causes an increase in the DOS of Mg_2Rh_3P. If we assume that Mg simply contributes electrons to the conduction band [20], we can derive the heat-capacity coefficient γ_{band} for SC-$Mg_{2-\delta}Rh_3P$ as $3.96\,\mathrm{mJ\,mol^{-1}\,K^{-2}}$, which is about 2.8 times larger than that of NS-Mg_2Rh_3P. We can estimate the mass enhancement factor as $\gamma_n/\gamma_{band} = 1.35$, which is quite reasonable for the mass enhancement by the electron–phonon interaction.

The Debye temperature $\Theta_D = 329$ K was derived using the formula $\beta = N(12/5)\pi^4 R\Theta_D{}^{-3}$, where $R = 8.314\,\mathrm{J/(mol\,K)}$ and $N = 6$ ($N =$ the number of atoms in the unit cell). The Θ_D was close to the value obtained by the resistivity fitting. According to the McMillan equation for electron–phonon-mediated superconductors [29], the electron–phonon coupling constant $\lambda_{e\text{-}p}$ can be determined by $\lambda_{e\text{-}p} = (\mu^*\ln(1.45T_c/\Theta_D) - 1.04)(1 - 0.62\mu^*)/(1.04 + \ln(1.45T_c/\Theta_D))$ where μ^* is a Coulomb pseudopotential parameter. Using $T_c = 3.86$ K, $\Theta_D = 329$ K, and the standard μ^* value (=0.13), we obtained $\lambda_{e\text{-}p} = 0.58$, indicating that SC-$Mg_{2-\delta}Rh_3P$ is a superconductor in the weak-coupling regime.

The inset in Fig. 7 shows the temperature dependence of $C_{el}/\gamma_n T$. The electronic specific heat C_{el} is obtained by subtracting the phonon part ($C_{ph} = \beta T^3$) from the total C. A clear jump of $C_{el}/\gamma_n T$ is observed at 3.8 K (the midpoint temperature of the jump), which is in good agreement with the values measured by magnetization and resistivity, indicating the bulk nature of the superconductivity. The dashed curve below T_c in the inset in Fig. 7 shows the T-dependent $C_{el}/\gamma_n T$ calculated using weak-coupling BCS theory. The normalized specific heat jump $\Delta C_{el}/\gamma_n T_c$ is estimated to be 0.72, which is only approximately half of the BCS value ($\sim$1.43). Furthermore, the experimental $C_{el}/\gamma_n T$ values show more moderate temperature dependence than that predicted by the BCS theory. These findings suggest that the size of the superconducting gap $\Delta(0)$ of SC-$Mg_{2-\delta}Rh_3P$ is much smaller than the BCS value ($2\Delta(0)/k_B T_c = 3.53$). In order to understand the superconductivity in SC-$Mg_{2-\delta}Rh_3P$ in more detail, specific-heat measurements at lower temperatures (<2 K) are required.

E. Pressure effects

The effects of pressure may help in enhancing T_c of SC-$Mg_{2-\delta}Rh_3P$ through the substitution of the constituent elements of the compounds. We applied physical pressure to SC-$Mg_{2-\delta}Rh_3P$ to reveal the effect of lattice compression on T_c. Figure 8 shows the temperature dependence of normalized magnetization for SC-$Mg_{2-\delta}Rh_3P$ as a function of applied pressure. T_c is observed to decrease with increasing pressure at a rate of approximately $dT_c/dP = -0.34$ K/GPa,

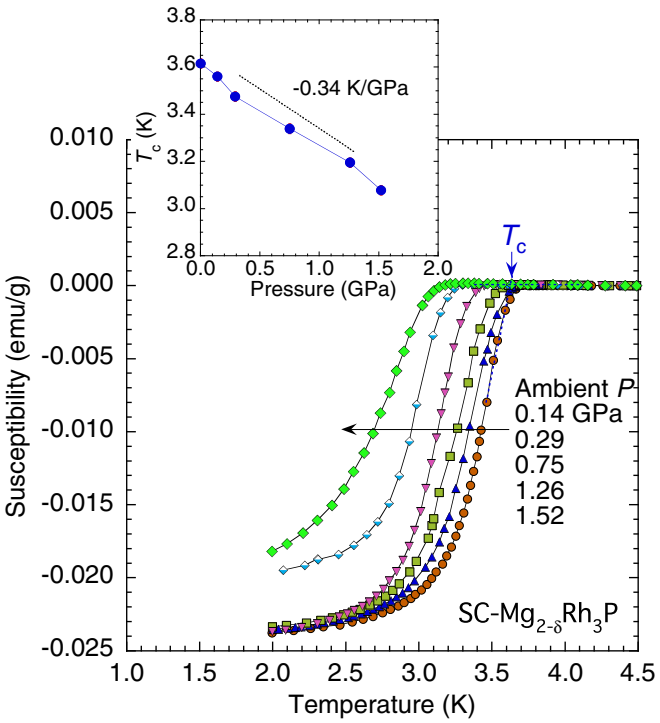

FIG. 8. Temperature dependence of magnetic susceptibility near T_c for the SC-$Mg_{2-\delta}Rh_3P$ sample, as a function of applied pressure (P). The inset shows the pressure dependence at the midpoint T_c.

as shown in the inset of Fig. 8. The decrease in T_c can be simply explained by a decrease in the DOS at E_F caused by the lattice size reduction under pressure. Conversely, T_c may increase if a lattice parameter increases by the chemical substitution of an element such as Ca for Mg. The volume of SC-$Mg_{2-\delta}Rh_3P$ was expected to decrease typically ∼1% by applying a pressure of 1.5 GPa. However, the decrease in volume by the Mg deficiency was only 0.067% (see Table II). The effect of volume shrinkage due to Mg deficiency on DOS should be negligible. Thus, the emergence of superconductivity in Mg_2Rh_3P (increase in DOS) is mainly attributed to the electron doping induced by the Mg deficiency.

F. Exotic fermions in Mg_2Rh_3P

Dirac fermions are found in many compounds and are attracting increasing attention. Dirac fermions carry topological charge and are considered useful for quantum calculation. In general, electrons in a crystal have lower symmetry than in free space. Because of this lowered symmetry, various quasiparticles that are prohibited in free space can exist. Bradlyn *et al.* recently proposed the presence of extremely anomalous quasiparticles such as threefold, sixfold, and eightfold degenerated states in some crystal structures [6]. Figure 9 shows part of the band structure of NS-Mg_2Rh_3P near the Fermi level. The crystal structure of the NS-Mg_2Rh_3P belongs to space group #212 or #213, which can have sixfold degenerated exotic fermions at the R(π/a, π/a, π/a) point [6]. Along the R–X axis, all the bands are doubly degenerated because of the crystal symmetry. Moreover, each band along this line forms a

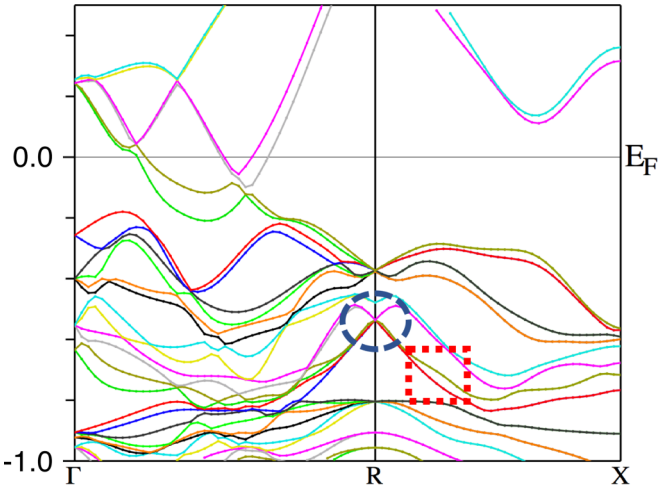

FIG. 9. Band structure near the Fermi energy (E_F) for NS-Mg_2Rh_3P. The unit of vertical axis is eV. The dashed circle shows the exotic fermion, which is the same type of quasiparticle as in Li_2Pd_3B [6]. The dashed square shows the band splitting arising from the lack of inversion symmetry and the spin-orbit interaction.

"pair." In the limit of zero spin-orbit interaction, this splitting becomes zero. The size of the splitting is seen, for example, in the dashed square in Fig. 9. As shown, the magnitude of this splitting depends on the wave vector, but we can estimate the average splitting is similar to that in Li_2Pd_3B [6] and much smaller than that in Li_2Pt_3B [22,30]. This result suggests that the parity mixing for the superconducting order parameter of SC-$Mg_{2-\delta}Rh_3P$ may not be so large, likewise in Li_2Pd_3B. The state at the R point is sixfold degenerated, and dispersion near this R point is approximately linear. This state may be observed by angle-resolved photoemission spectroscopy (ARPES) if a single crystal is obtained. Since this exotic fermion carries different topological charges than an ordinary Dirac fermion, if this state can be observed and controlled, it would be useful not only to explore novel physical properties, but also to create new types of topological quantum devices.

TABLE III. The physical parameters experimentally determined in this study for SC-$Mg_{2-\delta}Rh_3P$.

Parameters	Values in SC-$Mg_{2-\delta}Rh_3P$
T_c	3.9 K
H_{c1}	73 Oe
H_{c2}	24.3 kOe
λ_0	3010 Å
ξ_0	116 Å
κ_{GL}	26
γ_n	5.36 mJ mol^{-1} K^{-2}
β	0.328 mJ mol^{-1} K^{-4}
Θ_D	329 K
$\lambda_{e\text{-}p}$	0.58
$\Delta C_{el}/\gamma_n T_c$	0.72
dT_c/dP	–0.34 K/GPa

V. CONCLUSION

We succeeded in synthesizing the new ternary phosphide Mg_2Rh_3P, with the Al_2Mo_3C-type structure, in both superconducting and nonsuperconducting states. We demonstrated that the superconductivity of Mg_2Rh_3P is induced by Mg deficiency, and that the superconductivity can be controlled by the synthesis conditions, which may be useful in device fabrication. We revealed the basic physical parameters of SC-$Mg_{2-\delta}Rh_3P$, as summarized in Table III, together with a determination of its electronic structure. There are issues regarding the behavior of H_{c2} and the specific heat below 2 K that remain unanswered and require further study. Searching for new Mg_2Rh_3P-related compounds is also an interesting task left for a future study.

ACKNOWLEDGMENTS

This work was partially supported by JSPS KAKENHI Grants No. JP19K04481 and No. JP16H06439. We thank Editage (www.editage.jp) for English language editing.

[1] M. Smidman, M. B. Salamon, H. Q. Yuan, and D. F. Agterberg, Rep. Prog. Phys. **80**036501 (2017).
[2] F. Kneidinger, E. Bauer, I. Zeiringer, P. Rogl, C. Blaas-Schenner, D. Reith, and R. Podloucky, Physica C **514**, 388 (2015).
[3] M. Nishiyama, Y. Inada, and G.-q. Zheng, Phys. Rev. Lett. **98**, 047002 (2007).
[4] E. Bauer, G. Rogl, X.-Q. Chen, R. T. Khan, H. Michor, G. Hilscher, E. Royanian, K. Kumagai, D. Z. Li, Y. Y. Li, R. Podloucky, and P. Rogl, Phys. Rev. B **82**, 064511 (2010).
[5] A. B. Karki, Y. M. Xiong, I. Vekhter, D. Browne, P. W. Adams, D. P. Young, K. R. Thomas, Julia Y. Chan, H. Kim, and R. Prozorov, Phys. Rev. B **82**, 064512 (2010).
[6] B. Bradlyn, J. Cano, Z. Wang, M. Vergniory, C. Felser, R. Cava, and B. A. Bernevig, Science **353**, aaf5037 (2016).
[7] K. Momma and F. Izumi, J. Appl. Crystallogr. **41**, 653 (2008).
[8] J. Johnston, L. E. Toth, K. Kennedy, and E. R. Parker, Solid State Commun. **2**, 123 (1964).
[9] L. E. Toth, W. Jeitschko, and C. M. Yen, J. Less-Common Metals, **10**, 29 (1966).
[10] H. R. Khan, H. Trunk and CH. J. Raub, W. A. Fertig, and A. C. Lawson, J. Less-Common Metals **30**, 167 (1973).
[11] H. Yoshida, H. Okabe, Y. Matsushita, M. Isobe, and E. Takayama-Muromachi, Phys. Rev. B **95**, 184514 (2017).
[12] K. Togano, P. Badica, Y. Nakamori, S. Orimo, H. Takeya, and K. Hirata, Phys. Rev. Lett. **93**, 247004 (2004).
[13] U. Eibenstein and W. Jung, J. Solid State Chem. **133**, 21 (1997).
[14] P. Badica, T. Kondo, and K. Togano, J. Phys. Soc. Jpn. **74**, 1014 (2005).
[15] H. Niimura, K. Kawashima, K. Inoue, M. Yoshikawa, and J. Akimitsu, J. Phys. Soc. Jap. **83**, 044702 (2014).
[16] W. Wei, G. J. Zhao, D. R. Kim, C. Jin, J. L. Zhang, L. Ling, L. Zhang, H. Du, T. Y. Chen, J. Zang, M. Tian, C. L. Chien, and Y. Zhang, Phys. Rev. B **94**, 104503 (2016).
[17] Dassault Systèmes Americas Corp., BIOVIA Materials Studio Reflex website, https://www.3dsbiovia.com/products/collaborative-science/biovia-materials-studio/analytical-and-crystallization-software.html (accessed May 7, 2019).
[18] P. Blaha, K. Schwarz, G. K. H. Madsen, D. Kvasnicka, and J. Luitz, *WIEN2k, An Augmented Plane Wave + Local Orbitals Program for Calculating Crystal Properties* (Wienna: Vienna University of Technology, 2001).
[19] J. P. Perdew, K. Burke, and M. Ernzerhof, Phys. Rev. Lett. **77**, 3865 (1996).
[20] I. Hase, T. Yanagisawa, A. Iyo, H. Fujihisa, H. Eisaki, and K. Kawashima, J. Phys.: Conf. Ser. **1293**, 012028 (2019).
[21] H. Wiesmann, M. Gurvitch, H. Lutz, A. Ghosh, B. Schwarz, M. Strongin, P. B. Allen, and J. H. Halley, Phys. Rev. Lett. **38**, 782 (1977).
[22] E. Helfand and N. R. Werthamer, Phys. Rev. **147**, 288 (1966).
[23] N. R. Werthamer, E. Helfand, and P. C. Hohenberg, Phys. Rev. **147**, 295 (1966).
[24] A. M. Clogston, Phys. Rev. Lett. **9**, 266 (1962).
[25] B. S. Chandrasekhar, Appl. Phys. Lett. **1**, 7 (1962).
[26] K. Maki and T. Tsuneto, Prog. Theor. Phys. **31**, 945 (1964).
[27] G. Eguchi, D. C. Peets, M. Kriener, and Y. Maeno, E. Nishibori, Y. Kumazawa, K. Banno, S. Maki, and H. Sawa, Phys. Rev. B **83**, 024512 (2011).
[28] M. Isobe, K. Kimoto, M. Arai, and E. Takayama-Muromachi, Phys. Rev. B **99**, 054514 (2019).
[29] W. L. McMillan, Phys. Rev. **167**, 331 (1968).
[30] K.-W. Lee and W. E. Pickett, Phys. Rev. B **72**, 174505 (2005).